Analog Integrated Circuits and Signal Processing 3, 91–103 (1993)

Analog Circuits for a Single-Chip Infrared Controlled Hearing Aid

ALBERT C. VAN DER WOERD
Delft University of Technology, Department of Electrical Engineering, Electronics Research Laboratory, Mekelweg 4, 2628 CD Delft, The Netherlands

Abstract. All analog circuits for a remotely controllable subminiature hearing aid are presented. It is feasible to integrate all circuits together with an I^2L decoder on a single bipolar chip. The volume level and the cutoff frequency of a high-pass filter can be controlled. Besides, the device can be remotely switched at microphone and telephone coil, and switched into a standby mode. All circuits presented have been tested with a semicustom realization.

Received January 8, 1992; Revised May 19, 1992

1. Introduction

Because of its invisibility to others, most people with moderate hearing loss prefer a hearing aid that is mounted within the ear duct. As the small dimensions of such instruments obstruct the application of hand control, they must be remotely controlled. Three different systems for remote control in hearing aids are in use nowadays. They employ ultrasound, infrared, or radio frequencies as information carriers, respectively. Due to its insensibility for spurious signals and its quick response, an infrared system, such as that which has been applied for many years in consumer electronics, is probably the best choice.

This paper contains a description of all analog circuits for an infrared controlled hearing aid to be mounted within the ear duct. The digital part (I^2L decoder) is not described. The circuits have been designed for direct production purposes.

Figure 1 depicts a block diagram of the complete system. IR-modulated code words are received by a photodiode. Its signals are amplified and detected, after which they are decoded into digital current bits. These bits are converted into analog control currents controlling volume levels, filter transfers, and a standby position. A specification of the desired operation data and the boundary conditions is listed in Section 2.

The system contains a preamplifier with a doubled first stage. Hence signals from an electret microphone and from a telephone coil can be amplified separately. The amplified signals are filtered by a controllable second-order high-pass filter. At last the filtered signals are amplified to the desired level in a power amplifier. Furthermore, the block diagram contains a few reference sources. They are two PTAT current sources, a "hard" (low-ohmic) voltage source and a "soft" (high-ohmic) voltage source. The first PTAT source biases all circuits except the IR receiver. In the standby position this current source is switched off.

The second PTAT source biases the IR receiver that remains in operation during standby. The currents compensate for the temperature dependence of the controlled gain. The "soft" voltage source has yet another function, namely, it serves as a reference voltage for the "hard" voltage source.

2. Operation Data and Boundary Conditions

2.1. Control Functions

The infrared receiver receives repeated code words, amplitude modulated on a 36-kHz carrier, from a transmitter. The electronic circuits in the hearing aid must be able to react on each different code word in the following ways: The amplification must be controllable over a 46.5-dB range with steps of 1.5 dB. The filter circuit must have a second-order high-pass characteristic. Its cutoff frequency must be controllable over a range from 100 Hz to 1 kHz with eight steps (a low-pass function is not applied in this system, because for the majority of people with moderate hearing loss a high-pass function only is sufficient [1]).

Furthermore, the input transducer must be switchable from microphone to telephone coil, and vice versa. At last the total instrument except the IR receiver must be switchable from the operation mode to a standby mode, and vice versa. In the standby mode the power consumption should be minimized and the information in the (volatile) I^2L memories should be maintained.

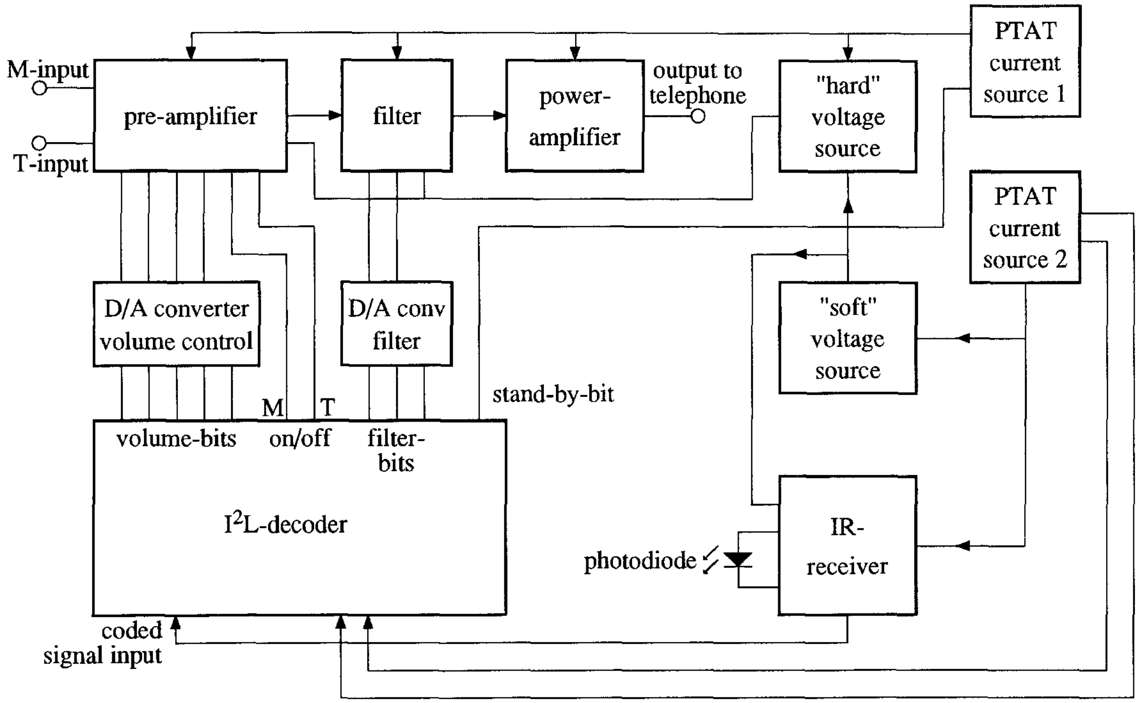

Fig. 1. Block diagram of the complete system.

2.2. *Transducers and Signal Levels*

The maximum power capability of the power amplifier must be 250 μW. This power must be delivered to a standard electromagnetic telephone, especially constructed for hearing aids. At that output level the input level of the preamplifier signal must be 150 μV_{rms} at maximum amplification. This input signal is delivered by a standard subminiature electret microphone with built-in junction FET or by a telephone coil. The output noise (unweighted and measured over a bandwidth of 10 kHz) of the microphone amounts to 13μV. This is a typical value for such microphones. At maximum gain the equivalent input noise of the controlled amplifier must be small with respect to that value. With decreasing gain an amplifier noise increasing to, say, 10μV will generally be admissible. The microphone signal can be as large as 35 mV. The controlled amplifier must be able to process such signals at low gain levels. The signal level at the connection between the controlled amplifier and the filter has been normalized at 15 mV_{rms} over 50 kΩ. Hence, the voltage gain must be controllable from -6.5 to 40 dB. The filter itself has a voltage gain of 6 db; hence, the output level at the connection of the filter and the power amplifier amounts to 30 mV_{rns}.

2.3. *Boundary Conditions*

a. All circuits must be designed with a single supply voltage of 1.0 V (zinc-air cell at end of lifetime).
b. As all circuits must operate at one very small zinc-air cell, total power consumption should be kept as low as possible (typically a few hundred microwatts, the power amplifer excluded).
c. Due to room problems, chip dimensions should be kept as small as possible. As an indication: A total chip area of 5 $\times$ 5 mm^2 will be too large.

3. General Design Aspects

3.1. *Process Choice*

Apart form the analog circuits, the chip must contain a large digital part and a number of D/A converters for the processing of the received infrared commands. An I^2L-compatible high-frequency process is chosen for the following reasons:

a. Available CMOS processes with very low threshold voltages (about $\pm$0.5 V) are not (yet) sufficiently characterized for analog applications in the production phase. Analog CMOS processes with higher threshold voltages are not suitable for the present application, unless a battery voltage multiplier is added to the circuit. This implies that an extra number of discrete capacitors is needed [2]. This is not feasible in the present application due to room problems.

b. As a large amount of the chip will be filled with I^2L gates for the digital processing, a realization in an I^2L-compatible (low frequency) bipolar standard process would give rise to too large chip dimensions for the present application. In high-frequency processes, however, special attention has been paid to minimizing the parasitic capacitances and delay times. Consequently, the minimum dimensions of bipolar devices generally are considerably smaller than in low-frequency processes [3]. Hence, owing to its large component density, the remaining possibility is an I^2L-compatible high-frequency process.

However, for the time being, all circuits in this paper have been designed for semicustom realization, in order to check their feasibility for production purposes.

4. Practical Circuits

4.1. The Infrared Receiver

Figure 2 depicts a block diagram of a practical IR receiver for hearing aids. the photo current is made free of dc current (caused by sunlight and artificial light sources) and other low- and high-frequency spurious signals by a dc killer and a bandpass filter. Thereafter

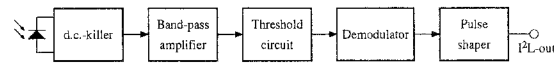

Fig. 2. Block diagram of the IR receiver.

the signal is connected to a threshold circuit. This circuit prevents false messages if the received signal is too weak. At last, the signal is detected and shaped.

Figure 3 depicts the circuit diagram. In traditional IR receivers direct currents are killed by an inductor. Of course, this must be rejected in the present application. Here the dc current is simply suppressed by a passive resistor (R_2). This measure affects the noise properties, and therefore the attainable distance range. However, this is not a large problem, because a distance range of, say, one meter will be sufficient. This range is fully feasible with the applied resistive dc killing, unless a fairly high transmission power is applied (the system was tested with a standard transmitter for TV remote control).

The maximum measured dc photocurrent under normal wearing conditions (photodiode in the ear duct) remains below 65 μA. The photodiode saturates, as soon as $V_{AK} > \approx +0.4$ V. Hence the value of R_2 has been chosen as large as possible (22 kΩ), so that the photodiode will never come into saturation ($I_{dc}R_2 < 1.4$V). However, under extreme conditions, for example when the device is placed in bright sunlight, the dc photocurrent can increase to 500 μA. Here a fundamental drawback of the circuit appears: Apart from the fact that the device cannot be controlled under such conditions, the battery will be discharged by the dc current.

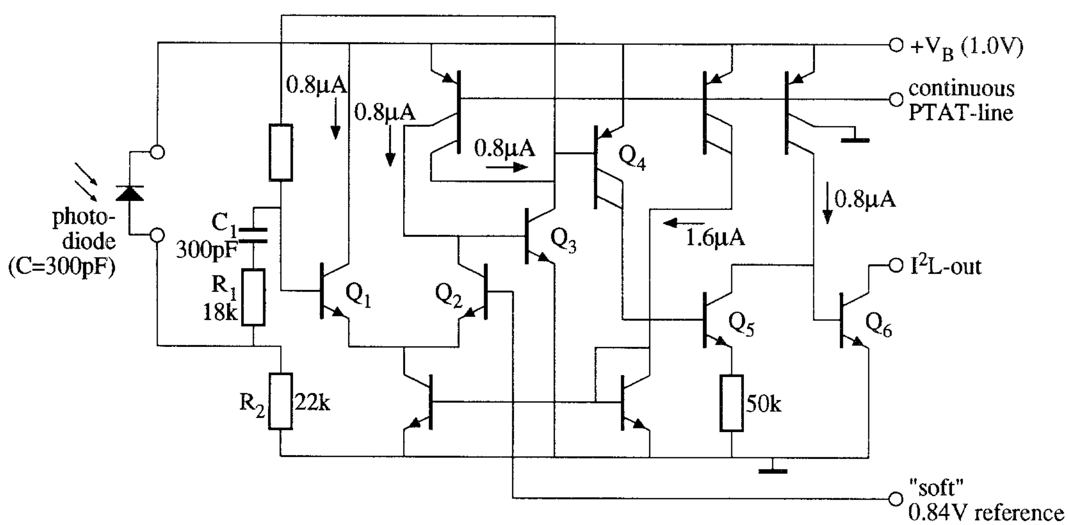

Fig. 3. Circuit diagram of the IR receiver.

In order to cope with this drawback, and to attain a higher sensibility, so that a smaller transmission power will be sufficient, the part of the circuit that is responsible for the dc killing has recently been redesigned [4]. In this new design *active* dc killing is applied (higher sensitivity), whereas the photodiode is kept *forward-biased*, so that dc currents do not discharge the battery. However, to the author's knowledge, it has never been applied in complete hearing aids until now.

The bandpass filter is realized by a capacitive-coupled amplifier with overall feedback ($Q_{1,2,3}$). The (first-order) low-pass function is realized by the coupling capacitor C_1 (300 pF), whereas the feedback amplifier operates as a second-order low-pass filter. We restrict ourselves to a rough description of the operating principle here. A more detailed description of the design aspects will be published in a subsequent paper.

The biasing currents of the transistors have been chosen to be 0.8 μA. At these bias currents the transfer shows two complex conjugate zeros and two complex conjugate poles, both at about 36 kHz. The positions of the zeros are the ends of the root locus. The positions of the zeros (and, therefore, the poles) can be influenced very effectively by resistor R_1. With $R_1 = 18$ kΩ the poles are arranged in the Bessel position (i.e., at frequencies of 36 kHz$(0.5\sqrt{3} \pm 0.5j)$.

The threshold circuit is formed by the (normally cutoff) transistor Q_4. At last, Q_5 and Q_6 operate as a pulse shaper, whereas their high input time constant suppresses the 36-kHz carrier as well (detection).

4.2. The Preamplifier with Its D/A Converter

4.2.1. General description. Figure 4 shows the block diagram of the preamplifier. In order to restrict distortion and power consumption, the total amplification control range is partitioned over three stages. The amplification steps are 24, 12, 6, 3, and 1.5 dB, respectively. For efficiency reasons the smallest steps (6, 3, and 1.5 dB) are controlled by the third stage. Both input stages control the 12-dB step, whereas the intermediate stage controls the 24-dB step. The actual control is effected by three transconductance amplifiers, mutually connected via current-to-voltage converters. The D/A converter converts the binary-coded volume level, the choice of the input transducer, and the operation mode into appropriate tail currents for the transconductance amplifiers.

Figure 5 depicts the circuit diagram of the preamplifier. The doubled first stage and the second stage contain traditional OTAs and need no further explanation. the third stage is controlled by its common emitter current too, but here the stage has been applied with two independent outputs. One output contains the amplified output current that will be connected to the filter circuit; the other output delivers a current for two offset-control circuits (for the microphone and the telephone mode, respectively), consisting of R_1, R_2, R_3, C_m, C_t, and the dc output resistances of the microphone/telephone coil. Hence, the capacitors C_m and C_t have two functions: dc decoupling and offset compensation.

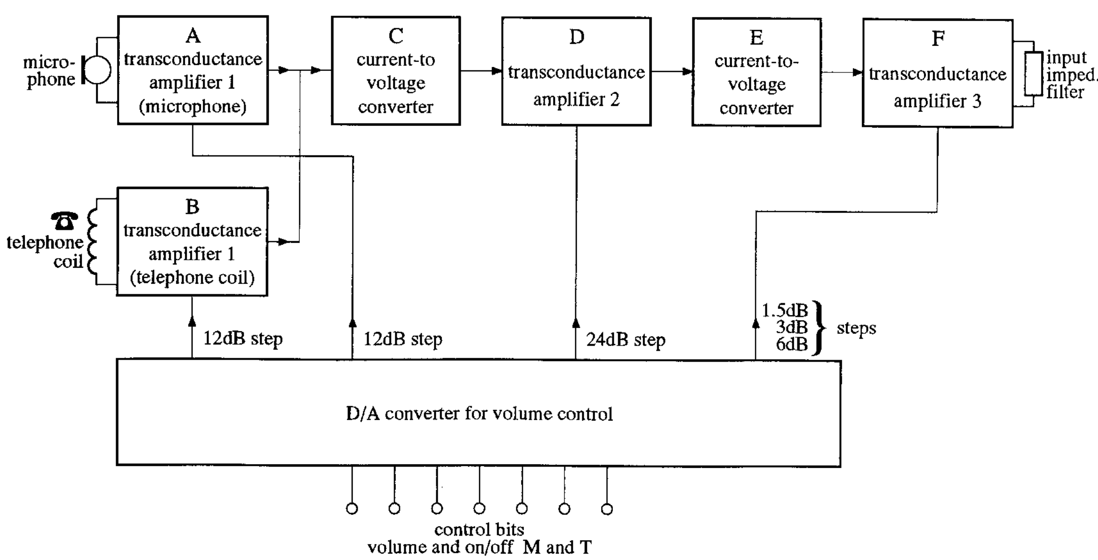

Fig. 4. Block diagram of the preamplifier with D/A converter.

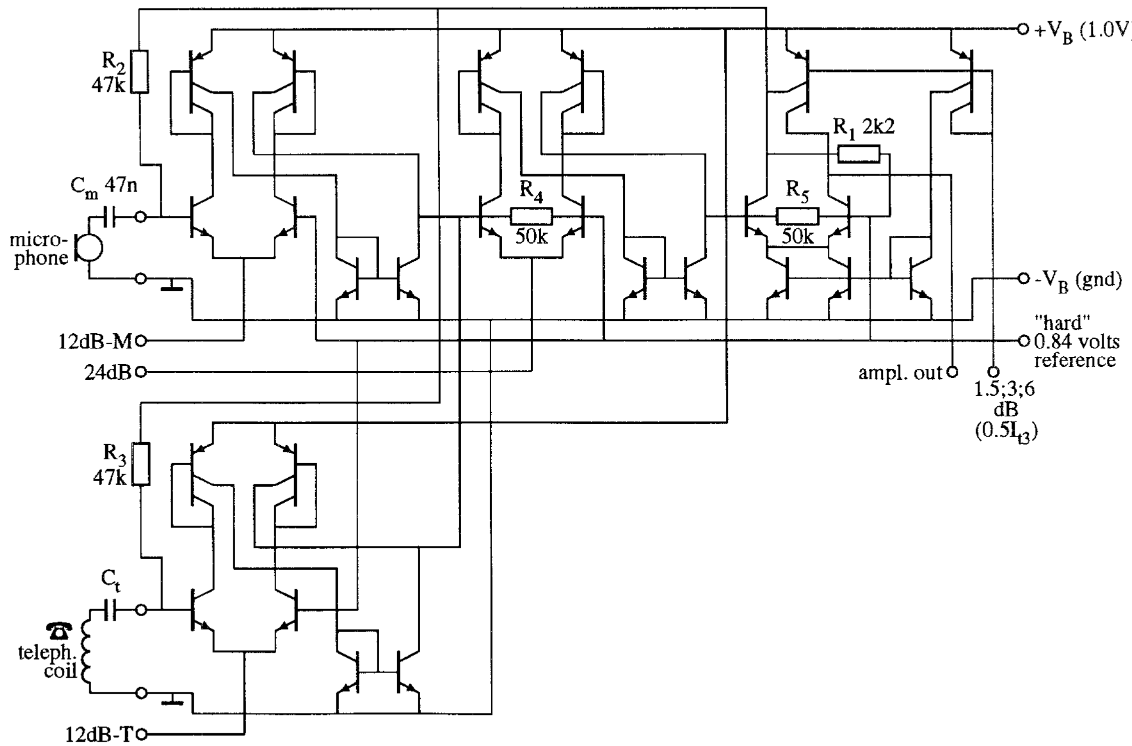

Fig. 5. Circuit diagram of the preamplifier.

As current-to-voltage converters, resistors have been applied.

4.2.2. *Voltage gain.* The voltage gain contributions of the first, second, and third stages are $I_{t(1)}R_4/2V_T$, $I_{t(2)}R_5/2V_T$, and $0.5I_{t(3)}R_G/2V_T$, respectively. The factor 0.5 is caused by the fact that the third stage is not loaded by a current mirror. Total voltage gain G_v from the input transducer to the input resistor of the filter circuit (R_g) amounts to

$$G_v = 0.5I_{t(1)}I_{t(2)}I_{t(3)}R_4R_5R_G/(2V_T)^3 \qquad (1)$$

where $I_{t(1)}$, $I_{t(2)}$, and $I_{t(3)}$ are the tail currents of the first, second, and third OTA, respectively, and V_T is the thermal voltage KT/q. In the microphone mode, the tail current of the telephone stage is made zero, and vice versa. In the standby mode the total amplifier is made current-free.

The amplifier gain is controlled by a combination of the three tail currents. In the control position where minimum gain occurs, the tail currents $I_{t(1,2,3)}$ amount to 0.8, 0.8 and 3.2 μA, respectively. At maximum gain these currents are 3.2, 12.8, and 8.8 μA, respectively. Hence, substituting the current and component values, and taking V_T = 25 mV, we obtain for the minimum and maximum gain

$$G_{min} = -5.8 \text{ dB} \quad \text{and} \quad G_{max} = 45.1 \text{ dB}$$

The upper gain value is somewhat too large. However, this is compensated by a small gain compression effect caused by the offset control. Due to the same effect the control curve shows a small nonlinearity. With the given component values of the offset control circuit in figure 5 this compression at maximum gain just equals 5 dB, so that the resulting gain limits passably fit the demands.

4.2.3. *Noise analysis.* In this section the noise properties of the preamplifier are analyzed and calculated. No weighting curve has been taken into account. Owing to the fact that the tail current of the third stage at least equals that of the first stage in any control position, the noise contribution of the third stage and the filter will be small (but not negligible) compared with those of the first and second stages. However, for the sake of simplicity the noise analysis only concerns the first two stages. Hence, the noise figures found will be somewhat too optimistic. (See the measuring results in Section 6.)

With the approximations mentioned above, the noise properties have to be analyzed in only four control

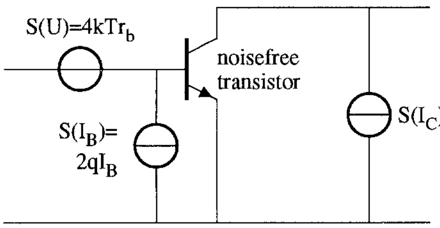

Fig. 6a. Noise sources in a BJT.

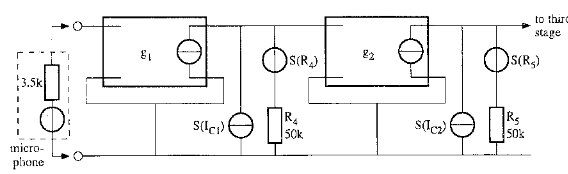

Fig. 6b. Block diagram for noise calculation.

positions, namely with the following combinations of the tail currents $I_{t(1)}$ and $I_{t(2)}$ of the first two stages:

$$\begin{array}{ll} (i) & (ii) \\ I_{t(1)} = 0.8\ \mu\mathrm{A} & I_{t(1)} = 0.8\ \mu\mathrm{A} \\ I_{t(2)} = 0.8\ \mu\mathrm{A} & I_{t(2)} = 12.8\ \mu\mathrm{A} \\ (iii) & (iv) \\ I_{t(1)} = 3.2\ \mu\mathrm{A} & I_{t(1)} = 3.2\ \mu\mathrm{A} \\ I_{t(2)} = 0.8\ \mu\mathrm{A} & I_{t(2)} = 12.8\ \mu\mathrm{A} \end{array} \tag{2}$$

As a start, the noise sources of a single bipolar transistor are given in figure 6a. Owing to the low values of the bias currents, the only relevant source is that, caused by the collector shot noise with spectrum $S(I) = 2qI_c$. Figure 6b depicts a block diagram of the first two stages with their (relevant) noise sources. the stages are considered as ideal resistor-loaded transconductance amplifiers. due to the symmetrical current-mirror loading, the spectrum of the collector shot noise is four times as large as in a single transistor. Hence, $S(I_c) = 8qI_c = 4qI_t$. The *current* spectrum of resistors R_4 and R_5 is $S_I(R_{4,5}) = 4kT/R_{4,5}$. The spectrum of the equivalent input noise voltage $S(U_{\mathrm{ieq}})$ can easily be found by applying simple noise transformation techniques [5]. The result is

$$S(U_{\mathrm{ieq}}) = \frac{4qI_{t(1)}}{g_1^2} + \frac{4kT}{R_4 g_1^2} + \frac{4qI_{t(2)}}{g_1^2 g_2^2 R_4^2} + \frac{4kT}{g_1^2 g_2^2 R_4^2 R_5} \tag{3}$$

where g_1 and g_2 are the transconductances of the first two stages. After substitution of all quantities for cases (*i*)–(*iv*) in (2), and calculating the r.m.s. input noise voltages $U_{\mathrm{ieq}}(\mathrm{rms}) = \{S(U_{\mathrm{ieq}})B\}^{1/2}$, where B is the signal bandwidth (=10 kHz), we obtain

$$U_{\mathrm{ieq}}(\mathrm{rms}) \approx 9,\ 6,\ 3,\ \text{and } 2.5\ \mu\mathrm{V, respectively.}$$

These values seem quite acceptable if they are compared with the output noise of the microphone.

Figure 7 shows the circuit diagram of the D/A converter. The switchable PTAT current is multiplied by such a number that the correct tail currents occur in any control step. Each tail current consists of the sum of a number of output currents from amplifying *NPN* current mirrors. Each current mirror can be switched off by short-circuiting its diode part.

4.3. The High-Pass Filter with Its D/A Converter

As the filter circuit is placed *behind* the controlled amplifier, only a minor noise contribution is acceptable. Therefore, it is not feasible to design a circuit with integrated capacitances in this system. Hence, two external capacitors have been applied.

Figure 8 gives the block diagram of the second-order high-pass filter. It contains two cascaded, capacitor-loaded gyrator sections. Each gyrator consists of two transconductance circuits ($G_{1,2}$ and $G_{4,5}$, respectively). Both gyrator sections are cascaded via a single transconductance circuit (G_3). If $G_1 = G_2 = G_4 = G_5 = G$, each gyrator circuit simulates an inductance

$$L_G = C_G/G^2 \tag{4}$$

Hence, the cutoff frequency of each filter section yields

$$f_c = R_G G^2/2\pi C_G \tag{5}$$

The filter shows two equal poles, whereas the transfer in the passband equals G_3. The cutoff frequency is controlled by varying the gyrator constant G.

Figure 9 shows the circuit diagram of the filter. It only contains single-ended transconductance stages. Hence, the relation between their transconductances G and their tail currents I_t equals

$$G = I_t/4V_T \tag{6}$$

where V_T (the thermal voltage) $= kT/q$.

All transistors are biased wth 0.8 μA. At minimum control current (0.8 μA) the cutoff frequency must be 100 Hz. Substituting $R_{G1} = 50\ \mathrm{k}\Omega$, $R_{G2} = 62.5\ \mathrm{k}\Omega$, $I_t = 1.6\ \mu\mathrm{A}$, and $kT/g = 25$ mV into (5) and (6), we obtain $C_{G1} \approx 13.2$ nF and $G_{G2} \approx 16.5$ nF.

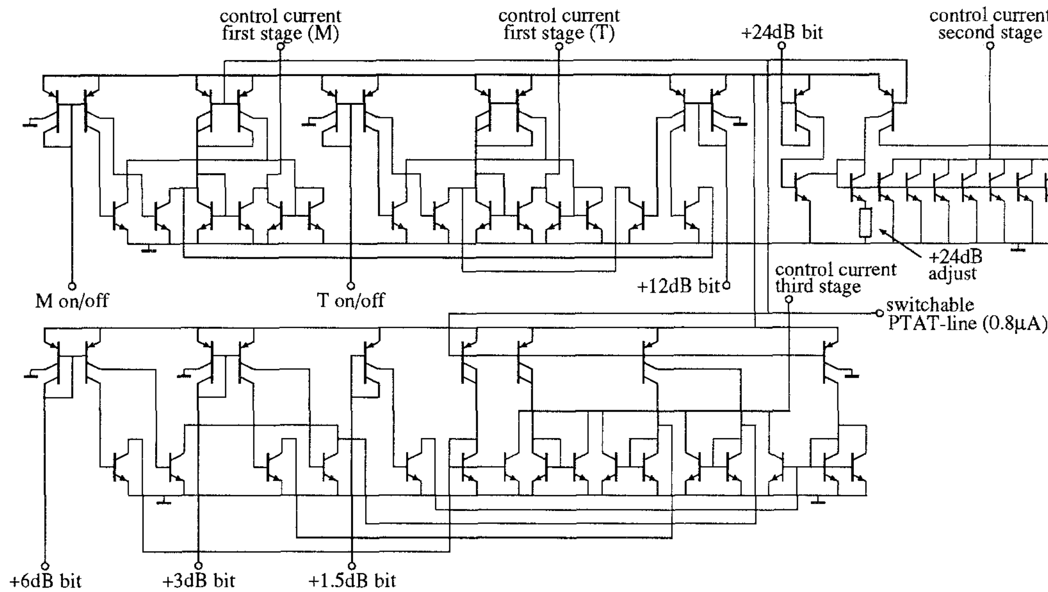

Fig. 7. Circuit diagram of the D/A converter for the preamplifier.

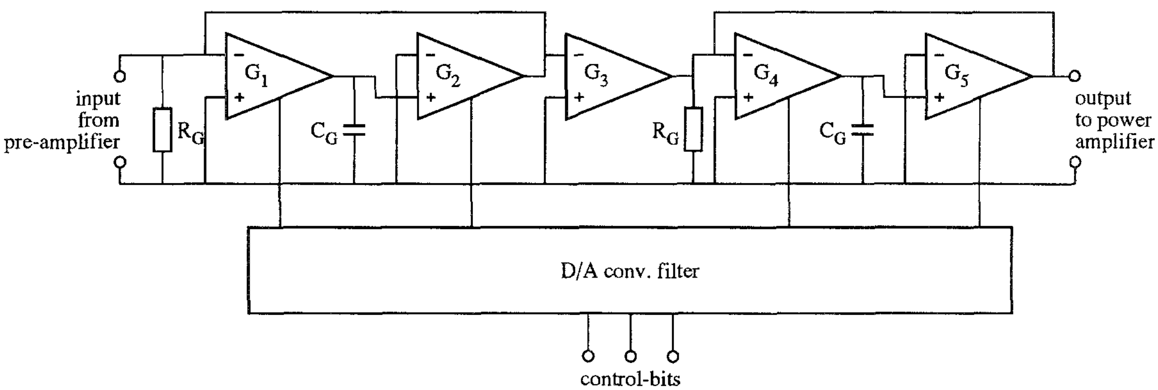

Fig. 8. Block diagram of the second-order high-pass filter.

The D/A converter that delivers the control current operates according to the same principle as that of the controlled preamplifier. Therefore, no circuit diagram has been added. It is arranged in such a way that the control current is proportional to the binary value of the input signal. Hence, according to (4) and (5), the cutoff frequency of the filter is a quadratic function of the control current. Such a control characteristic appears to be convenient in practical use.

Both gyrator stages show a transfer of 0 dB in the passband, while the gain contribution of the intermediate stage (G_3) has been chosen at 6 dB. Hence the signal level at the filter output is 30 mV over 62.5 kΩ at maximum gain.

4.4. *The Voltage References*

Figure 10 depicts the circuit diagram of the "soft" and the "hard" voltage references. The "soft" voltage delivers a rather high ohmic voltage of about 0.84 V and consists of a cascade of a diode and four saturated *NPN* transistors with "forced beta." A formula for the calculation of the saturation voltage (V_{sat}) of a BJT is

$$V_{sat} = I_C R_C + \frac{kT}{q} \ln \left(\frac{1 + 1/B_i + B_n/B_i(I_C/B_i I_B)}{1 - I_C/B_n I_B} \right) \tag{7}$$

where R_C is the collector bulk resistance, B_n is the forward dc current gain and B_i is the inverse dc current

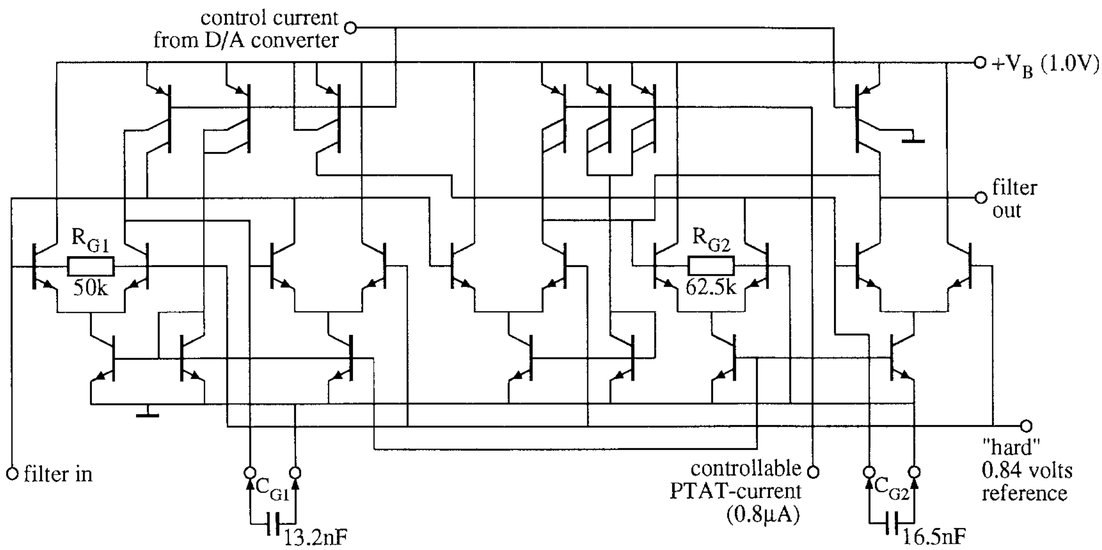

Fig. 9. Circuit diagram of the second-order high-pass filter.

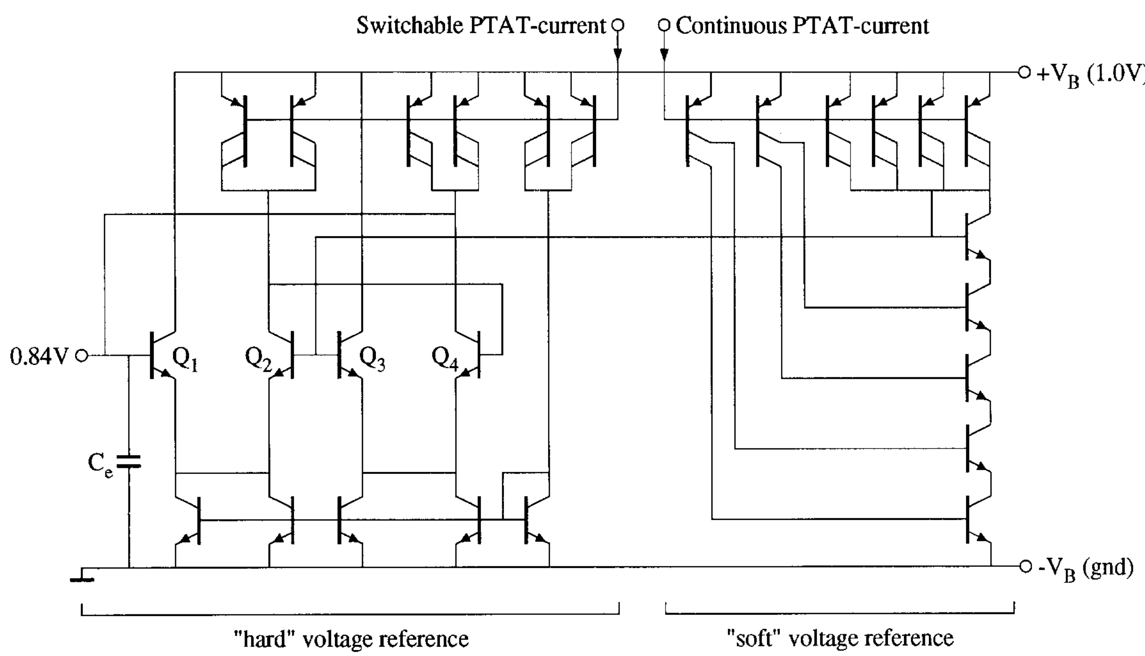

Fig. 10. Circuit diagram of the "soft" and "Hard" voltage references.

gain. Formula (7) can easily be derived from the equations of the Ebers-Moll model [6]. The continuous PTAT current amounts to 0.8 μA. Hence, the saturated transistors of the soft voltage reference are biased with currents varying from 6.4 to 8.8 μA. With such small currents the effect of R_C can be neglected. Hence, if the relation I_C/I_B is kept constant, the saturation voltage only depends on B_n, B_i, and temperature. (It is independent of the supply voltage.) Theoretically it is perfectly PTAT, unless the effect of R_C is absent.

Comparisons between measuring a calculation results have shown differences in V_{sat} up to 20%. Obviously, the employed transistor models were not adequate for the present application. Therefore, the composition of the saturated transistors and their I_C/I_B ratios have been experimentally designed for the time being. To get an impression of the accuracy of V_{sat} in practice, 10 arbitrarily chosen samples of the compete semicustom realization were subjected to measurements. The resulting values of the soft reference voltage varied from 0.826 to 0.847 V with an average of 0.840 V and a standard deviation of 5 mV. The hard reference voltage varied from 0.824 to 0.845 V with an average of 0.838 V and a standard deviation of 6 mV. We have paid no attention to temperature effects, because they are of minor importance in hearing aids. Finally, the supply voltage dependence of the hard reference was measured. As a result, a power source rejection ratio of 44.7 dB was found.

On the one hand, the soft voltage reference serves as a reference voltage for the IR receiver; on the other hand, it serves as a reference voltage for the hard voltage source. In the stand-by mode the soft reference remains in operation, whereas the hard reference is switched off. The hard reference contains a voltage follower with two stages (the differential pairs $Q_{1,2}$ and $Q_{3,4}$). Its dc output impedance is about 1.5 kΩ. This is sufficiently low to prevent relaxation effects in the total system. The external capacitor C_e ensures high-frequency stability and prevents additional noise. C_e is a microminiature elco of 3.3 μF.

4.5. *The Current References*

Apart from the possibility to switch off the current in the standby mode, both current sources are identical and deliver a current of about 1 μA. In the complete system the sources are loaded by numerous *PNP* transistors. Consequently, the ultimate currents decrease to ≈ 0.8 μA.

Figure 11 shows the switchable source. The actual PTAT source has been designed according to [7]. The capacitor C_C (30 pF) prevents the circuit from high-frequency instability. As such sources show two stable operation modes, a starting circuit must be added. This is realized by adding a starting current of 1 nA to the circuit, delivered by the resistor R_s and the downscaling current mirror $Q_{2,1}$. This starting current is used for both current sources, but it has yet another function. Two currents of 1 μA and 1 nA, respectively, delivered by Q_4 and Q_5 are used as a bias current and a standby current for the I^{2}L decoder. Hence, the information of the control functions is maintained during standby, whereas the power consumption of the I^{2}L decoder in the standby mode is minimized. The source is switched off in the standby mode, where Q_6 is short-circuited. The employed switching circuit is the same as it is used in the D/A converters (figure 7).

4.6. *The Power Amplifier*

Figure 12 depicts the circuit diagram of the (class A) output amplifier. It contains three stages, accomplished by transistors $Q_{1,2}$, Q_3, and Q_4, respectively. The feedback network is formed by $R_1 + R_2 + r(Q_3)$ and R_a. The maximum output power level can be adjusted by

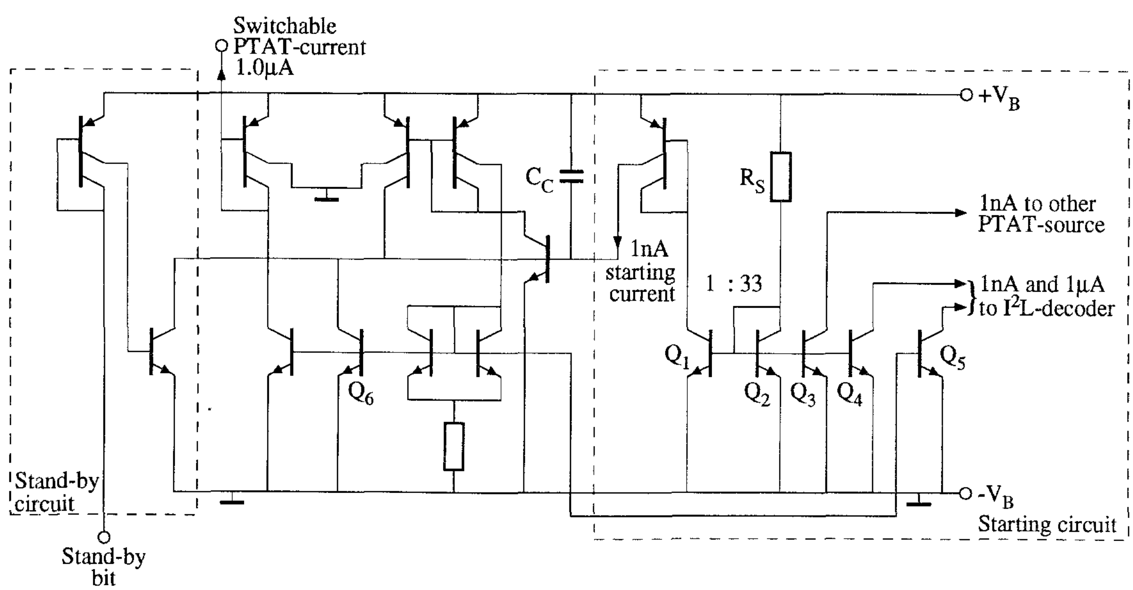

Fig. 11. Circuit diagram of the switchable PTAT current source.

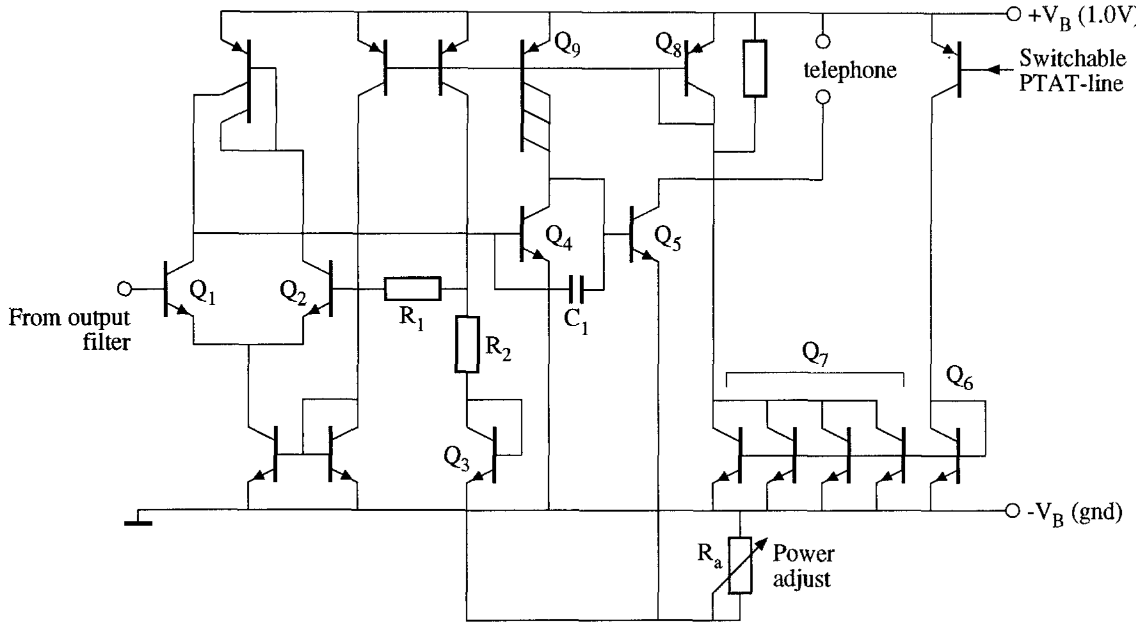

Fig. 12. Circuit diagram of the power amplifier.

R_a. The total amplifier can be made free of bias current by switching off the switchable PTAT current (standby mode). High-frequency stability is ensured by the pole-splitting capacitor C_1. Apart from the possibility of a standby mode, the power amplifier circuit is traditional. Therefore, no further details are given.

5. Semicustom Realization

In order to check their feasibility for production purposes, all circuits presented have been realized on two chips in a semicustom process. Figure 13 shows photomicrographs of the chips. The ultimate full-custom chip, where the circuits together with the I^2L logic have been integrated, cannot be shown for confidential reasons.

6. Simulation and Measuring Results

In this section the simulation and measuring results of the preamplifier and the filter circuits will be shown. Further some figures concerning distortion, power consumption and offset will be given. Some measuring results concerning the voltage references have been given in Section 4.4. For measuring and simulation results of the current references, we refer to [7].

6.1. The Preamplifier

Figure 14 depicts the simulated and measured maximum and minimum preamplifier gain. Total control area amounts to 46 dB. From detailed measurements of the gain as a function of the binary control input from 00000 through 11111, it has been shown that the resolution remains <1.5 dB in any control step. Both graphs for minimum and maximum gain show different corner frequencies. At minimum gain the high-frequency roll-off as well as the low-frequency roll-off lie at lower frequencies than at maximum gain. The change in the low-frequency roll-off is caused by the offset control, whose loop gain increases at higher gain steps. The high-frequency roll-off is higher at maximum gain than at minimum gain, because the OTAs get larger tail currents. Between the lowest step and the highest step the bandwidth will show various values, depending on the binary input word. However, the worst case is attained at minimum gain. Even in this situation the bandwidth is much larger than needed ($\gg 10$ kHz). One could suggest that bandwidth could be exchanged with supply power so that the upper frequency limit would be restricted to 10 kHz. However, this would be disastrous for the noise properties. The part of the bandwidth above 10 kHz must be considered as an accidental circumstance neither necessary nor harmful.

Within the signal bandwidth (100 Hz–10 kHz) the measuring point fit well with the simulation results. At

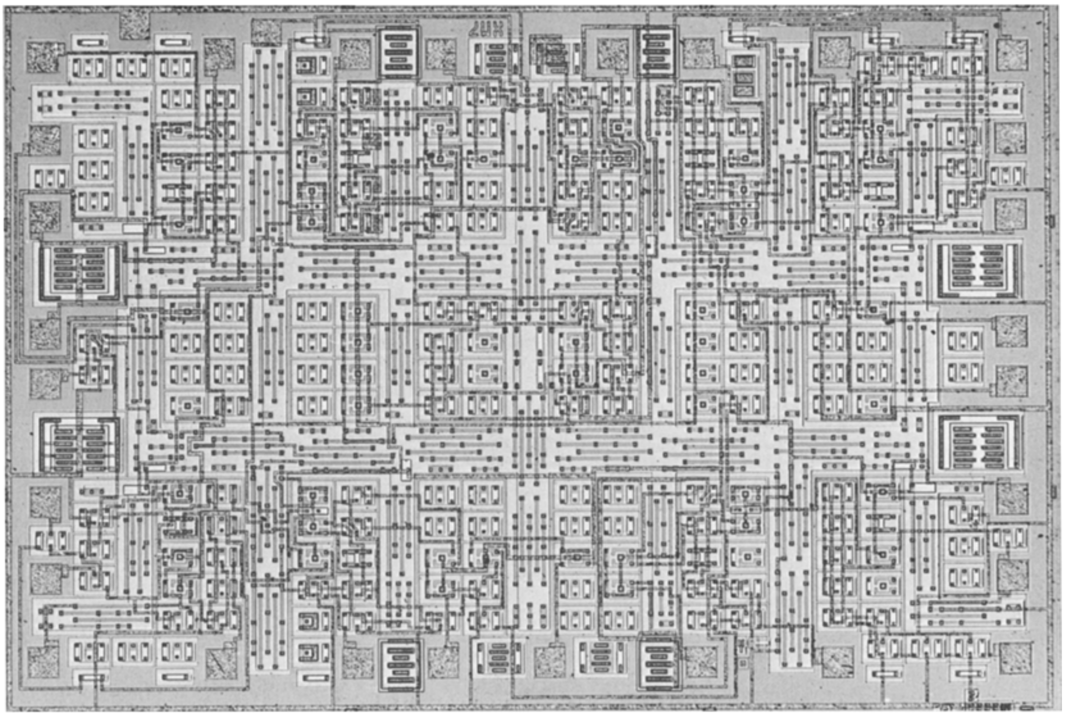

(a)

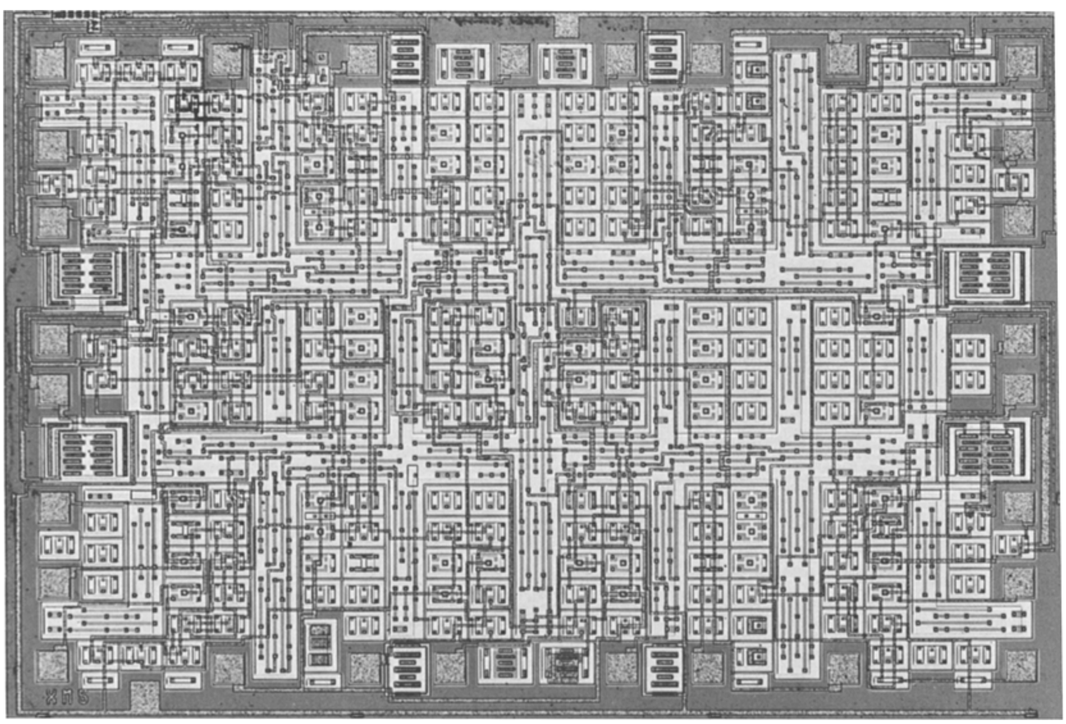

(b)

Fig. 13. Photomicrographs of both semicustom chips.

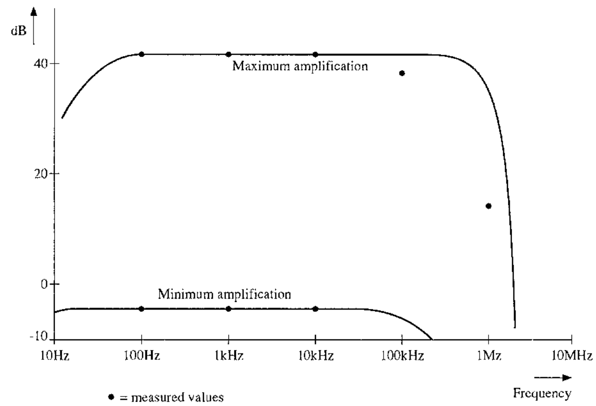

Fig. 14. Simulated and measured maximum and minimum preamplifier gain.

higher frequencies, however, a considerable deviation occurs. We suppose that this is caused by inadequate high-frequency characterization of the employed transistor models at very low bias currents. Due to the minor importance for the present design, we paid no further attention to this phenomenon.

6.2. The High-Pass Filter

In figure 15 the filter transfers at minimum and maximum cutoff frequency are depicted. The filter behaves as expected. Indeed, its corner frequency can be varied between 100 Hz to 1 kHz, whereas its transfer in the passband remains fairly constant. Within the signal bandwidth the simulation results fit very well with the measuring points. At higher frequencies considerable differences occur. For an explanation of this phenomenon we refer to Section 6.1.

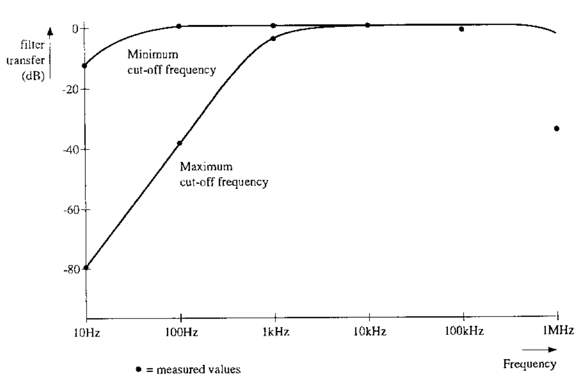

Fig. 15. Simulated and measured filter transfers.

6.3. Noise Measurements

Figure 16 shows the measured r.m.s. noise voltage at the output of the filter divided by the voltage gain (equivalent input noise) as a function of the controlled gain. No weighting function has been applied, whereas a bandwidth of 10 kHz has been taken into account. The maximum signal voltage level at the filter output is 30 mV_{rms} at maximum gain. Curve A gives the noise contributions of the preamplifier-filter combination *without* microphone, Curve B gives the microphone noise only. During the measurements, the filter cutoff frequency was set at 100 Hz. In that position the noise contribution of the filter is maximum (smallest control currents) hence, the worst-case situation has been measured. Comparing the results with the calculated values (Section 4.2.3), we observe that the measured values are somewhat worse than the calculated values. This affirms the supposition made in Section 4.2.3, that the noise contributions of the third stage of the preamplifier and the filter cannot be disregarded. The graphs show that the noise, added by the circuitry, is quite acceptable in any control position.

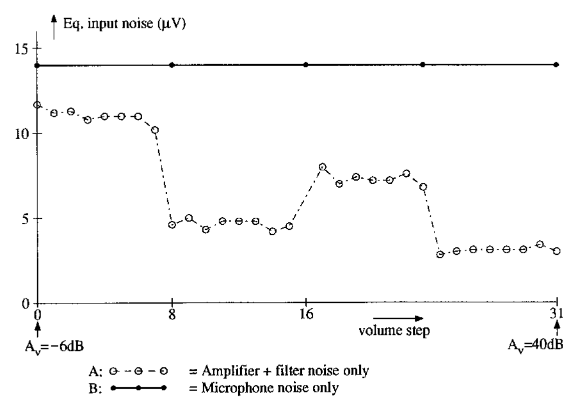

Fig. 16. Measured r.m.s. input noise voltage (nosie voltage at the output of the filter divided by the voltage gain) as a function of the controlled gain. Curve A: contribution of the amplifier + filter; Curve B: contribution of the microphone only.

6.4. Distortion, Power Consumption, and Offset

The measured total harmonic distortion at full output level is less than 7% in any control position. This is sufficiently low for the present application. The measured total supply power (the power amplifier *included*) amounts to 1.05 mW (at a supply voltage of 1.0 V). Offset is mainly caused by transistor mismatch and finite base currents. In order to get some impression of practical offset figures, the offset voltage at the output of the filter was measured with 10 arbitrarily chosen samples of the semicustom realization. The maximum and minimum offset values amounted to -1.19 mV and -3.78 mV with a standard deviation of 0.764 mV.

7. Conclusions and Suggestions

All analog circuits for a single-chip remotely controllable hearing aid have been proposed. The system contains an infrared receiver, a preamplifier for an electret microphone or a telephone coil, a second-order high-pass filter, a power amplifier, and the necessary voltage and current references. The gain of the preamplifier and the cutoff frequency of the filter can be controlled by binary code words. Besides, the system can be switched into a standby mode with a single bit. The feasibility of all quality demands has been demonstrated. Therefore, first production experiments are believed to be fully justified.

Although all specifications needed can be realized, some properties can be considerably improved. They are listed below.

a. Using other principles for the controlled amplifier, the filter circuit and the power amplifier (class B), the simplicity, efficiency, and noise properties of the total system can be greatly improved.
b. The infrared receiver can be improved so that dc spurious signals do not discharge the battery and less transmission power is sufficient [4].

Research is going on to realize the improvements mentioned above. The results will be published in subsequent papers.

References

1. G. Keller and L. Plath, *Technische Hilfe bei der Rehabilitation Hörgeschädigter*, Springer-Verlag: Berlin and New York, 1980.
2. F. Callias, F.H. Salchli, and D. Girard, "A set of four ICs in CMOS technology for a programmable hearing aid," *IEEE J. Solid-State Circuits*, Vol. 24, No. 2, pp. 301-312, 1989.
3. H.C. de Graaf and F.M. Klaassen, *Compact Transistor Modelling for Circuit Design*, Springer-Verlag: New York, Chap. 11, 1990.
4. A.C. van der Woerd, "Low-voltage low-power infra-red receiver for hearing aids," *Electron. Lett.*, Vol. 28, No. 4, pp. 396–397, 1991.
5. E.H. Nordholt, *Design of High-Performance Negative Feedback Amplifiers*, Elsevier: Amsterdam, Chap. 4, 1983.
6. I.E. Getreu, *Modeling the Bipolar Transistor*, Elsevier: New York, Section 2.2, 1978.
7. H.C. Nauta and E.H. Nordholt, "New class of high-performance PTAT current sources," *Electron. Lett.*, Vol. 21, No. 9, pp. 384–386, 1984.

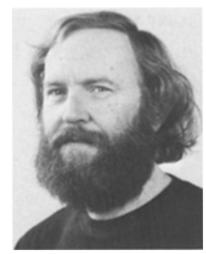

Albert C. van der Woerd was born in 1937 in Leiden, The Netherlands. In 1977 he received the Ir-degree in electrical engineering from the Delft University of Technology, Delft, The Netherlands. He was awarded the Ph.D. degree in 1985. From 1959 to 1966 he was engaged in research on and development of radar and TV circuits with several industry laboratories. In 1966 he joined the electronics research laboratory fo the Department of Electrical Engineering of the Delft University of Technology. During the first 11 years he carried out research on electronic musical instruments. The next 8 years his main research subject was on carrier domain devices. The last years he has specialized in the field of low-power/low-voltage analog circuits and systems. He teaches design methodology.